Sensing and Bio-Sensing Research 32 (2021) 100421

Contents lists available at ScienceDirect

Sensing and Bio-Sensing Research

journal homepage: www.elsevier.com/locate/sbsr

Mathematical characterization of ink diffusion and imbibition processes in chromatography paper as a potential biosensing platform

V.A. Mirón-Mérida *, M. Wu, Y.Y. Gong, Y. Guo, M. Holmes, R. Ettelaie, F.M. Goycoolea *

School of Food Science and Nutrition, University of Leeds, Woodhouse Ln, LS2 9JT, Leeds, United Kingdom

ARTICLE INFO

Keywords:
Chromatography paper
Mathematical model
Wicking
Diffusion

ABSTRACT

Materials used for biosensor development normally include silicon, glass, and synthetic polymers, however, paper is a practical and cheap option for the reduction of manufacturing costs with a wide range of applications. Paper-based biosensors have been widely produced, yet poorly characterized on the interaction of different type of molecules with its intricate microstructure. In this work, five ink solutions were prepared as model samples to examine their diffusion and imbibition behavior on grade 3MM chromatography paper. Different mathematical models, previously reported for porous matrices, were fitted and results revealed that upward wicking ($r^2 \geq 0.90$) equations described the experimental data during the initial stage (< 5 s) and yielded similar permeability values to those calculated from the matrix structural properties. The diffusion coefficient was determined up to attaining equilibrium using the diffusion equation in a cylinder element ($r^2 \geq 0.90$). This study enabled the characterization of the performance from 3MM chromatography paper, by using ink as a surrogate model of small molecules (e.g. mycotoxins) or small colloidal particles.

1. Introduction

Many concepts have been utilized for describing transport phenomena in porous media, which can be regarded as physical complex processes including convection, diffusion, imbibition and heat transfer, where the permeability of the porous medium has a strong influence on these phenomena and their time evolution [1]. Likewise, imbibition is a relevant concept to different fields ranging from petroleum and civil engineering, geophysics, everyday commodities (tissues, paper rolls), and of course, paper-based chromatography and biosensing techniques [2,3]. From the different material supports in biosensing, paper represents an attractive option, given its amenability for the development of fast, affordable and versatile assays, thus offering the possibility of identifying diverse targets. Paper-based biosensors are commonly designed as dipsticks, lateral flow tests, or paper-based analytical devices (μPADs) [4], in which nitrocellulose is commonly utilized as the platform for the development of different signals. For instance, colorimetric determinations through the conjugation of gold nanoparticles (AuNPs) with antibodies, for the single [5,6] and multiplex quantification of compounds [7], the application of aptamer-functionalized AuNPs [8], and the completion of chemical reactions [9,10] have been proposed as paper-based methods. The versatility and biocompatibility of paper have been exploited for the application of chemiluminescent compounds, substrates and quantum dots, resulting in the fabrication of single chemiluminescence (CL) [11], multiplex CL [12] and luminescent [13] assays, respectively. Other innovative measurements include paper separation coupled with electrochemical analysis [14], and the integration of surface-enhanced Raman scattering (SERS) on paper test lines [15]. Therefore, understanding the diffusive and capillary effects controlling the mobility of samples is a relevant step during the design and construction of a paper-based biosensor.

Due to is fibrous nature, paper is a porous medium, where it has been predicted that water first moves into the pores by covering the fiber surface and moving into them, followed by the occupancy of the inter-fiber pores. This penetration process is faster when following the fiber direction along the plane to that in the perpendicular direction [16]. Studies focused on inkjet ink for coated paper have demonstrated that after the ink drop is applied on the paper surface, the initial movement is generated by inertia. Then, a quick competition takes place against spreading and the capillary forces integrating the ink into the porous structure. In a matter of milliseconds, ink separation is also observed, followed by adsorption within ~1 s. Although diffusion appears with the first manifestations of capillary imbibition, the diffusion effect is more notorious as the penetration of ink increases (~10 s). The last stages

* Corresponding authors.
E-mail addresses: fsvamm@leeds.ac.uk (V.A. Mirón-Mérida), f.m.goycoolea@leeds.ac.uk (F.M. Goycoolea).

https://doi.org/10.1016/j.sbsr.2021.100421
Received 10 September 2020; Received in revised form 7 April 2021; Accepted 12 April 2021
Available online 16 April 2021

during inkjet printing are polymerization (~100 s) and drying (~1 h); however, these are usually not described during modelling. The given times are related to an onset point of such phenomena, as in reality, all of them coexist on the same porous matrix [17]. As observed in coated paper, small quantities of binder can affect the final rate of progress balance between the wetting force and the viscous drag, commonly denoted by the Young-Laplace Eq. [18]. At the initial stages of ink absorption in coated paper, imbibition is determined by the pore diameter, as capillary forces moved the liquid sample towards the coating area [19]. This process is followed by diffusion due to wettability and swelling [19]; nevertheless, this whole mechanism might differ in uncoated paper.

In general terms, the flow of liquid samples in a porous media such as paper, is driven by capillary forces occurring at the air-liquid interface, whose curvature and differences in surface tension produce the transport of samples, in a process commonly defined as passive pumping [20]. Furthermore, the flow of samples within porous paper channels regarded as capillary tubes, has been described as a correlation of the penetration distance and the time, described by Washburn equation, also referred as Lucas-Washburn equation (Eq. 1):

$$L(t) = \sqrt{\frac{r t \gamma cos\theta}{2\mu}} \tag{1}$$

Where L is the penetration distance, r is the average pore radius (capillary radius), γ is the surface tension, θ is the capillary wall-liquid contact angle, and μ the dynamic viscosity. For this estimation of the unidirectional penetration, the porous medium is addressed as an intricated array of tubes, where the channel width does not affect the travelled distance. Yet, as the wetting front is positively proportional to the square root of the pore radius, a faster imbibition profile would be expected for large capillaries [21–25]. The latter has been contradicted by studying the impact of geometric sectioning on a porous medium for the asymmetric capillary flow of samples in a lateral flow arrangement, in which narrowed sections had a quicker movement [21]. This entails that liquids tend to fill the finer pores within a paper layer, while inertia effects arise from large pores and a viscosity regulated absorption, commonly overlooked in Lucas-Washburn [16,24]. In this regard, the flow of samples can be manipulated, as proven by a cheap hybrid system combining digital microfluidics for the controlled incorporation and movement of samples with a 3MM chromatography paper μPAD on a lateral flow detection system [26]. In some other studies, the radial penetration of different compounds was recorded on filter paper under fluorescent light, where two drop-phases were identified before and after total penetration in the porous substrate, through a microlenses equipped videocamera [22]. Filter paper was also used for the fabrication of pumps, where the passive pumping effect produced by capillary forces denoted a linear correlation between a greater flow rate and an increasing sector angle [20]. Sample spreading in paper can be also accomplished by numerical simulations after obtaining a micro-tomography of the porous media with further validation of the droplet penetration by confocal microscopy [16]. Pore-scale two-phase simulations were also carried out by combining ion beam scanning electron microscopy with confocal laser microscopy validation [27]; however, both approaches analyzed such phenomena in a picoliter scale, with a highly controlled dosage of the selected model sample. Besides, many of these estimations require complicated computational and experimental settings [28], which only account for small sample volumes under different conditions misrepresenting the final biosensing approach and its wettability implications.

The Lucas-Washburn equation can be modified to fulfil the added effects of inertia, gravity, evaporation, and tortuosity [3]. Similarly, although imbibition corresponds to the transport of fluids in the x, y and z directions, the Lucas-Washburn equation can be adjusted to the kinetics of radial penetration, in which the transport of fluids is mainly measured along the y-direction [22,24]. The radial imbibition in a porous medium was analyzed in glass microspheres, in contact with a hole at the top of a container filled with wetting liquid. The analysis of the hemispherical front was explained with an expanded version of Darcy's law for a radial flow, with an integration of Laplace pressure [29] (Eq. 2).

$$r_f = A^{1/3} t^{1/3} \tag{2}$$

Where, $A = \left[\frac{3Kp_c r_s}{\mu}\right]^{1/3}$, $p_c = \frac{2\gamma cos\theta}{r_p}$ (Laplace capillary pressure), K, r_s, r_p, θ, γ and μ represent the permeability, initial front radius, pore radius, contact angle, surface tension and dynamic viscosity of the liquid, respectively, and t is time.

Likewise, wicking experiments performed on the upward propagation of hexadecane in cellulose webs confirmed the time-dependence of the liquid front point with a simplified version of Darcy's law with Lucas-Washburn Eq. [30], given as (Eq. 3)

$$L^2 - l_0^{\,2} = \alpha^2 (t - t_0) \tag{3}$$

Where, $\alpha^2 = D$, $\alpha = \sqrt{\frac{2p_C K}{\mu\Phi}}$, $p_c = 2\gamma/r_p$, p_c = capillary pressure, Φ = porosity of material, t_o is initial time, l_0 is the value of L at initial time, t is time, and D is the diffusion coefficent.

Additionally, capillary imbibition assays on filter paper revealed the influence of the matrix geometry on the mathematical models for describing fluid transport [31]. A radial cylindrical flow through a trapezoidal strip was calculated with the following equation (Eq. 4):

$$\frac{(1+al)^2}{2}\left[ln(1+al) - \frac{1}{2}\right] + \frac{1}{4} = a^2 Dt \tag{4}$$

where $a = 1/r_0$, $l = r\text{-}r_0$, r_0 = radius of the initial wetted area at $t = 0$. While a radial spherical flow through a non-linear cross-sectional area was predicted by eq. 5:

$$\frac{1}{6}\left[(1+al)^3 - \frac{1}{2}\right] - \frac{1}{2}\left[(1+al)^2 - 1\right] = a^2 Dt \tag{5}$$

Both equations derived from a combination of mass conservation expressions of Darcy's law, and a subsequent simplification by integrating Lucas-Washburn equation under different geometrical cross-sectional areas [29]. In all the previously mentioned models, Darcy's law has been used for denoting the single-phase spontaneous imbibition within porous media, while neglecting the viscosity of air and the gravitational effects [28].

Thus far, the assessment of the diffusion and capillary properties of paper-based systems have required especial cameras, lightning, reservoirs, chambers, or supports with multiple layers. Nevertheless, the application of real samples must be kept as simple as possible, and a better understanding of the diffusive and imbibition nature of paper under realistic circumstances must be gleaned. Furthermore, as most of the research has been focused on dipstick and lateral flow arrangements, μPADs are of particular interest, especially given that the applications of higher volumes (40–70 μL) take place on the central zone of the μPADs [10,32,33]. In this work, the diffusion of commercial blue ink (a mixture of pigments, glycerol and surfactants) used as a surrogate of small molecules (e.g., mycotoxins), was studied on 3MM chromatography paper. To this purpose, different mathematical models were examined to describe the radial flow of ink in porous media at short times. Similarly, a diffusion equation for a cylinder was fitted to the whole process to calculate the corresponding apparent diffusion coefficients. The application of ink was selected to simplify the experimental set up by utilizing the easily observable ink front.

2. Materials and methods

2.1. Materials

Chromatography paper grade 3MM, filter paper grades 1 and 540 were acquired from Whatman™ (UK). Permanent marker (Medium Point 1.0 mm Write-4-All Pen Permanent – Black) and stamp pad blue ink without oil were purchased from Stabile (UK) and Pelikan® (Germany), respectively. All the solutions were prepared with MQ water.

2.2. Methods

2.2.1. Preparation of ink models

Five samples were prepared through aqueous dilutions of blue stamp pad ink from Pelikan at 10, 25, 50, 75 and 100% (*w*/w) –where 100% corresponds to the undiluted ink.

2.2.2. Rheological determinations of the ink models

The rheological properties of the ink models were determined using a Kinexus rotational rheometer (Malvern, UK), fitted with a stainless steel double gap measuring system (C25 cylinder) for measuring the dynamic viscosity (η) at different shear rates ($\dot{\gamma}$).

2.2.3. Density of the ink models

The density values (g/cm^3) of the five ink dilutions were measured in an Anton Paar Density Meter DMA 4500 M, based on the oscillating U-tube method, with a calibration density check for water.

2.2.4. Interfacial tension of ink models

Interfacial tension measurements were performed at 20 °C in an OCA 25 instrument, by analyzing a 10 μL drop shape according to the pendant drop method. In the aforementioned method, a spherical liquid drop will be formed on a dosing needle (ø = 0.911 mm) due to the surface tension and gravity and can be analyzed with the Young-Laplace equation (Eq. 6) where Δp is the pressure difference through the fluid interface, γ is the surface tension, R1 and R2 the radii of curvature (Fig. S1a).

$$\Delta p = \gamma\left(\frac{1}{R1}+\frac{1}{R2}\right) \tag{6}$$

2.2.5. Contact angle of the ink models

The contact angle was measured at a contact line produced by an ink solution drop deposited on Whatman cellulose chromatography paper grade 3MM. According to the scalar Young equation:

$$\sigma_L \cos\theta_c = \sigma_S - \sigma_{SL} \tag{7}$$

where the contact angle (θ_c) is influenced by the vectorial equilibrium between the forces acting along the solid surface (σ_S), in opposite direction to the liquid-solid interface (σ_{SL}) and the liquid surface (σ_L) tension operating tangentially to the surface (Fig. S1b).

2.2.6. Porosity of paper

Prior to the porosity experiments, the paper samples were left in a desiccator containing 500 g of fully dried silica gel (SiO_2) for 24 h. The porosity measurement was obtained by the liquid displacement method [34], in which a 3MM chromatography paper square (V paper = 2 × 2 × 0.034 = 0.136 cm^3) was placed in a falcon tube containing 20 mL of absolute ethanol (ρ = 0.791 g/mL) for 48 h. Weights of the paper samples were recorded at different stages in order to obtain the volume (V) of impregnated ethanol after removal of the paper piece from the falcon tube. The porosity (ε) was calculated according to eq. 8.

$$\varepsilon = \left(\frac{V\ impregnated\ ethanol}{V\ paper}\right) \tag{8}$$

2.2.7. Scanning electron microscopy and pore size determination in paper

The surfaces of dry 3MM chromatography paper were coated with a thin layer of iridium (4 nm) with a sputter coater Essington 208HR, and scanning electron microscopy images were obtained with a FEI Nova NanoSEM 450 operating at 3 kV. The average pore diameter of the observed fibers was calculated in image J, by calibrating the SEM images in μm/pixel.

2.2.8. Application of the ink models on paper

Prior to the mathematical fitting assays, 50 μL from each ink model were vertically applied on the center of chromatography paper grade 3MM squares (4.5 × 4.5 cm), fixed with masking tape to a horizontal metallic base. The ink front was recorded with a mobile phone (IPhone 6 s plus), and the circular area at different times was calculated with Image J, from which the front radius/distance was obtained.

2.2.8.1. Diffusion coefficient estimation in chromatography paper. The mathematical fitting for the diffusion in a cylinder was performed in Origin Pro 8.6 32 for all the experimental data until a constant area was reached, as stated in eq. 9 [35] .

$$l_{rel} = \frac{l_t - l_0}{l_\infty} = \frac{4}{\pi^{\frac{1}{2}}}\left(\frac{Dt}{a^2}\right)^{1/2} - \frac{Dt}{a^2} - \frac{1}{3\pi^{1/2}}\left(\frac{Dt}{a^2}\right)^{3/2} \tag{9}$$

Where l_{rel} is the relative distance; l_t, l_0 and l_∞ are the front ink distance at a time *t*, at time 0, and at the equilibrium time, respectively. *D* represents the diffusion coefficient (m^2/s), *t* the diffusion time, and *a* is the radius achieved at the equilibrium stage.

2.2.8.2. Mathematical fitting of the radial flow in chromatography paper. Further mathematical model fittings of the recorded data were conducted in Origin Pro 8.6 32 Bit (2012) software, for eqs. 2, 3, 4, and 5 at short times (5 s), and their corresponding permeability values (experimental permeability) were calculated by integrating the measured parameters (contact angle, surface tension, viscosity, density) with the fitted values.

2.2.8.2.1. Permeability determinations for model selection. The experimental properties of 3MM chromatography paper (pore radius and porosity) were integrated to calculate the theoretical permeability (*K*), according to eq. 10, also known as the Kozeny-Karman model [29].

$$K = \frac{dm^2}{180}\frac{\varepsilon^3}{(1-\varepsilon)^2} \tag{10}$$

Where *K* = permeability, *dm* = diameter of pores, ε = porosity.

This equation derived from a more general approach for the calculation of the permeability in fibrous media described in eq. 11 [36].

$$K = \frac{dm^2}{36k}\frac{\varepsilon^3}{(1-\varepsilon)^2} \tag{11}$$

Where *k* isr the Kozeny-Karman constant, previously calculated for monodispersed fibers in a random packing arrangement [37]. In the case of Eq. 10, the *K* constant for beds packed with spherical particles was approximated to 5 [36], hence a value of 180 was estimated for this expression.

Another expression for permeability (*K*) was reported by Callegary and collaborators for the analysis in ultra-fine cellulose webs [30] as indicated in eq. 12.

$$K = r^2\frac{\varepsilon}{4k} \tag{12}$$

Where r = capillary radius, and *k* = Kozeny-Karman constant measured as already mentioned [37].

The three expressions of the Kozeny-Carman model for the permeability of porous media were selected as theoretical values for the further comparison with the experimental permeability data and selection of the best descriptor of the ink movement in paper at short times (5

s).

2.2.8.2.2. Comparison of Lucas-Washburn equation with its modified expressions. An exploration of different versions of the Lucas-Washburn equation was completed by fitting eq. 13 and eq. 14 to the recorded front ink distance at given time t ($t \leq 5$ s). The first model followed a nonlinear relation between l^2 and t, as denoted in eq. 13 [23,38].

$$l^2 = D^*t \tag{13}$$

From which D could express the effect of either the pore radius as traditionally represented in Lucas-Washburn ($D = r\gamma\cos\theta/2\mu$) [21,23] or nongravitational effects by integrating Darcy's law in substitution of Hagen-Poiseuille eq. ($D = 2C\varepsilon\cos\theta/S(1-\varepsilon)\mu$) [38]. Furthermore, the exploration of inertia effects provided by the density of samples, was indicated as the linear relation between l and t in eq. 14 from Schoelkopf [17].

$$l = D^*t \quad \text{where, } D = \sqrt{2\gamma cos\theta/r\rho} \tag{14}$$

A validation step was carried out between the fitted and expected D values, where the latter were obtained through the integration of the average pore radius (r) of the paper matrix, in combination with the surface tension (γ), contact angle (θ), viscosity(μ) and density (ρ) of the ink models, as expressed in each case.

3. Results and discussion

3.1. Diffusion coefficient estimation in chromatography paper

A preliminary selection of the paper matrix was performed through the application of aliquots of diluted pure ink on Whatman filter paper grades 1, 540, and Whatman 3MM chromatography paper. Despite the greatest area achieved with filter paper, the sample mobility on Whatman grade 1 and 540 was not adequate for accomplishing a homogenous spreading, as the pore size (11 μm particle retention) allowed penetration of the sample and some stained areas were found beyond the hydrophobic barriers (created according to Fig. S2). Hence, the rest of the study was carried out with Whatman 3MM chromatography paper. The diffusion through the porous layer of filter paper does not necessarily represent a negative attribute. In fact, this behavior has been exploited in the multiplex detection of DNA by paper-origami mechanisms [39].

The choice of colored blue ink was convenient for the simplification of the experimental settings and the ease to quantify its diffusion using image analysis techniques. To this end, a distinct circular front area was tracked using a mobile phone camera, without the aid of structural layers or external light sources. As displayed in Fig. S3, the area increment for the five ink models was plotted during 600 s, in which an increasing ink concentration led to a delay in reaching the steady stage, where a higher ink percentage was related to a greater front area. The physical properties of the five ink models are presented in Table 1. Note that an increasing ink percentage led to increasing viscosity and density values, and a decreasing interfacial surface tension (IST). On the other hand, although some reported wetting angle values for filter paper were equivalent to 89.84° [20]; in this work, the measured contact angle was zero, as revealed by the absence of drop formation on the porous substrate produced by the immediate absorption of the ink drop (Fig. S1d). This result was indeed expected, as a contact angle of zero is mainly produced by the hydrophilic nature of the fibers in contact with water, for that reason many printing papers and similar surfaces are treated and coated to increase the contact angle. In the case of untreated chromatography paper, a null contact angle implies greater spreading and penetration lengths [16].

Table 1
Physicochemical characterization of the five ink models.

Ink Concentration (%, v/v)	Density ρ (g/cm^3)	Dynamic viscosity μ (Pa s)	Contact angle Θ (°)	Interfacial surface tension γ (N/m)
10	1.0022	0.0012	0	0.0529
25	1.0148	0.0015	0	0.0475
50	1.0329	0.0021	0	0.0496
75	1.0527	0.0030	0	0.0493
100	1.0741	0.0047	0	0.0440

Ink diffusion on paper has been regarded as a Fickian process, in which migration takes place due to a concentration gradient triggered by Brownian motion [17]. Data fitting for Eq. 9 was applied to all the experimental points (Fig. S4) until diffusion equilibrium (constant area) was reached. The equilibrium times varied depending on the ink model and were equivalent to ~10, ~20, ~150, ~300, and 300 s for the various ink samples at increasing concentrations (10 to 100%). As illustrated in Fig. 1a, the selected mathematical expression was a good descriptor of the variability of the experimental data set, which was confirmed by the high determination coefficients ($0.93 < r^2 < 0.96$) for the calculated D values (Fig. 1a inset), and the linearity of the fitting curves between the mathematical and the experimental L_{rel}. In addition, as displayed in Fig. 1b, the calculated D values diminished with a rising ink concentration, which suggested a positive effect from the water content on the rapid achievement of a constant phase. Such impact on the diffusion coefficients (D), was expected after considering the effects from the physicochemical parameters of the ink models, mostly related to the composition of the stamp pad ink (21% glycerol, 16% sorbitan monooleate ethoxylated, 9% diethylene glycol, 6% pigment and 48% water). In this regard, an increasing viscosity combined with a decreasing surface tension have been previously related to a reduction in spreading and infiltration. Likewise, a higher density is expected to portray a slower imbibition performance [40], which is consistent with the results in this work. (See Fig. 1.)

The mathematical expressions describing the relation between the numerical (L_m) and the experimental (L_{rel}) relative distance for each ink

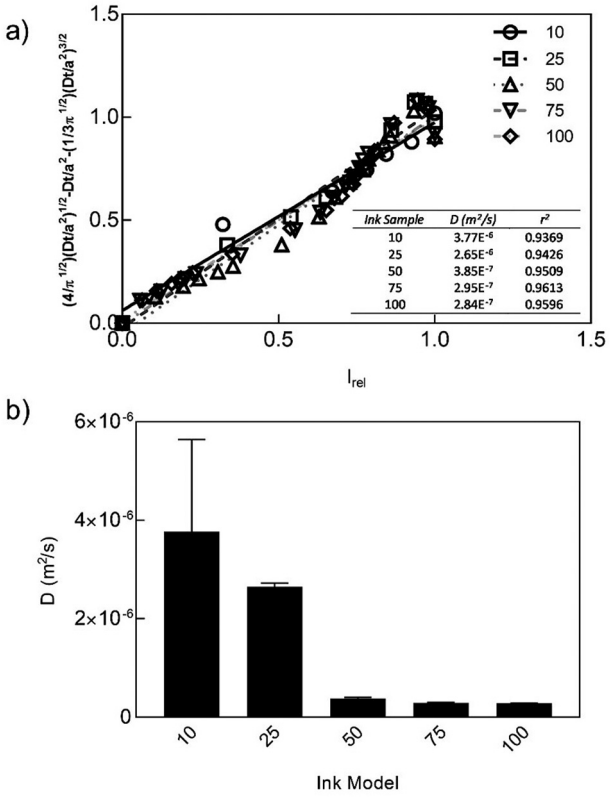

Fig. 1. (**a**) Calculated relative distance (l_{rel}) from Eq. 9 as a function of the experimental values and (**b**) its corresponding diffusion coefficients (D).

model, are indicated in Table 2. The satisfactory coefficients of determination ($r^2 = \sim 0.96$) demonstrated a good prediction of such linear relation, which can be also implied from the slope values in each equation ($y = mx + b$), where "m" was noticeably close to 1 for all the ink concentrations. A statistically significant correlation ($p < 0.05$) was found among the experimental and numerical relative distances, as revealed by the correlation coefficients ($R = \sim 0.98$) in Table 2.

Apart from the effects of the physical parameters inherent to the applied sample, an important consideration for the mathematical modelling of ink diffusion on paper is the industrial nature of chromatography paper. The fluid's displacement velocity has been proven to be also dependent on the cellulose microfiber's microscopic arrangement. This feature is uncontrollably developed during paper production, where the fibers are oriented either in the production machine or the cross direction, thus limiting the speed of liquid penetration [41]. A faster diffusion occurs in a parallel direction to the fibers, and when such diffusion is measured as parallel to the paper plane, the calculated coefficients are an average of all the fiber orientations. Moreover, this bulk behavior is observed in porous substrates at short times, whereas long-time approximations consider the connectivity of the porous network [42].

3.2. Permeability comparison for equation fitting of radial penetration models

The SEM images for 3MM chromatography paper are shown in Fig. 2a, in which a fibrous morphology was observed, similar to other porous uncoated cellulose-based materials where the fibers constitute their surface [33]. Although channel discontinuity and variable channel widths are normal for this kind of matrix [23], a continuous profile of homogenous cylindric fibers is assumed for the mathematical fitting of radial penetration models as displayed in Fig. 2b. Therefore, an average of 40 fiber width measurements from Fig. 2a (200 μm scale) were recorded to estimate the pore diameter, whose value was equivalent to 13.86 ± 4.14 μm, equal to approximately the double of the already reported particle retention value (6 μm) for 3MM chromatography paper [43]. In this regards, approximating the porous medium to a cylindrical capillary is a common strategy to simplify the penetration modelling, where the equivalent radius and equivalent contact angle are needed, yet the latter is commonly referenced as zero [38]. This value is also applied in the equation for capillary pressure (p_c) for upward wicking (Eq. 3), where $\cos\theta$ was not included [30], and complies to the observed results in the physicochemical characterization (Table 1). (See Fig. 3.)

Furthermore, the constants and r^2 values for eqs. 2, 3, 4 and 5 are indicated in Table 3, in which all the selected mathematical functions exhibited high determination coefficients (r^2) upon data fitting during the first 5 s. Some considerations for the application of such models are worth of note, namely the Stoke regime conditions such as stationary flow, absence of inertia, low Reynold numbers, and isothermal state [31]. Other assumptions included a small liquid source, uniform radial velocity, a radial pressure gradient, and predominance of the capillary pressure over the hydrostatic pressure [29].

Table 2
Mathematical expressions and correlation between the calculated relative distance (Lm) and its corresponding experimental value (Lrel).

Ink Concentration (%, v/v)	Equation	r^2	Correlation Coefficient R	*p*
10	Lm = 0.9129 Lrel +0.0615	0.964	0.9819	$8.43e^{-5}$
25	Lm = 1.0612 Lrel −0.0224	0.9667	0.9832	$3.40e^{-7}$
50	Lm = 1.0536 Lrel-0.0496	0.9659	0.9828	$3.61e^{-13}$
75	Lm = 1.011 Lrel −0.0068	0.9641	0.9818	$1.01e^{-13}$
100	Lm = 0.9788 Lrel+0.0127	0.9613	0.9804	$1.94e^{-13}$

The physical properties of the ink models (Table 1) and coefficients shown in Table 3 were integrated to estimate the experimental permeability(k). This variable was used as a reference parameter for comparing different mathematical approaches, as calculating the permeability rendered a way to converge different experimental inputs in one specific estimation. A theoretical permeability was considered after replacing some terms in the Kozeny-Karman model [36] and its two variations [29,30], whose approach related the pore structure to the permeability when using the measured pore diameter (13.86 μm) and porosity ($84.41 \pm 4\%$) for 3MM chromatography paper. The estimated porosity value used in the Kozeny-Karman model for this work, closely matched the porosity of 83% reported for cellulose nanowebs [30]. Different studies described porosities ranging between 31 and 41% for foxing-free and foxed paper samples, a general 70% porosity for paper [44], and 26.9, 68.2 and 63.7% for paper board, Whatman 1 filter paper and blotting paper, respectively [45].

Based on the plotted results in Fig.. S5 and their mathematical expression for determining the k constant as a function of the porosity [37], the Kozeny-Karman constant was calculated as 4.246, which was lower than the value of 5 utilized for spherical particles in Eq. 10 with a corresponding permeability of 2.63×10^{-11} m^2 [29]. This constant (4.246) was substituted in Eqs. 11 and 12 [30,36], which in combination with the pore radius/diameter and the porosity derived in permeabilities of 3.10×10^{-11} and 2.38×10^{-12} m^2, respectively. As demonstrated in Table 3 and Fig. S5, the theoretical values from the Kozeny-Karman model in eqs. 10 and 11, yielded comparable magnitudes to the permeability expressed from the curve fitting of upward wicking (Eq. 3) to experimental data. The Kozeny-Karman theoretical permeability showed an order of magnitude larger than previous values reported for cellulose acetate nanowebs ($k = 1.1 \times 10^{-13}$ m^2) [30], yet closer to the reported 1.21×10^{-12} m^2 for a porous medium made of soda lime glass microspheres in a box [29]. Despite the observed slight decrease on the diffusion coefficients, which, by formula, could be associated to viscosity increments and a decrease in the interfacial surface tension in a range from 25 to 100% (v/v) ink, the D value obtained from eq. 3 could be considered as a fairly constant parameter. Besides, the permeability results (K) indicated a homogeneous permeability from 25 to 75% ink, with a good approximation to the theoretical calculation (Fig. S6). It is worth mentioning that the diffusion coefficients shown in Fig. 1a (inset) were similar in order of magnitude to some of the D values calculated from eq. 4 (Table 3) for the cylindrical flow in porous media, which corresponds with the selected mathematical expression (Eq. 9) also describing the diffusion process in a cylinder. Nevertheless, based on the permeability value approximation, as wicking was the most suitable model for explaining the radial movement of the ink models on 3MM chromatography paper, it can therefore be argued that within 5 s passive pumping occurred due to capillary forces leading the flow of the models into the porous system [45]. In this regard, liquid spreading occurs as both a non-diffusive regime regulated by inertia, gravity and capillarity and a diffusive regime controlled by diffusion of the sample molecules [17], hence both determinations of diffusion (section 3.1) and radial penetration are pertinent for the selected material.

3.3. Comparison of Lucas-Washburn equation with its modified expressions

Previous studies have utilized Lucas-Washburn equation for explaining the flow of liquids in porous supports such as paper, and it has been demonstrated that this equation alone was not suitable for describing the flow in porous media and membranes at microscale [23]. By contrast with the Lucas-Washburn model, the modified equation has been suitable for describing the liquid flow in 3MM chromatography paper strips, with a greater consistency after more wetting-drying cycles were repeated [41]. However, as previously mentioned, Lucas-

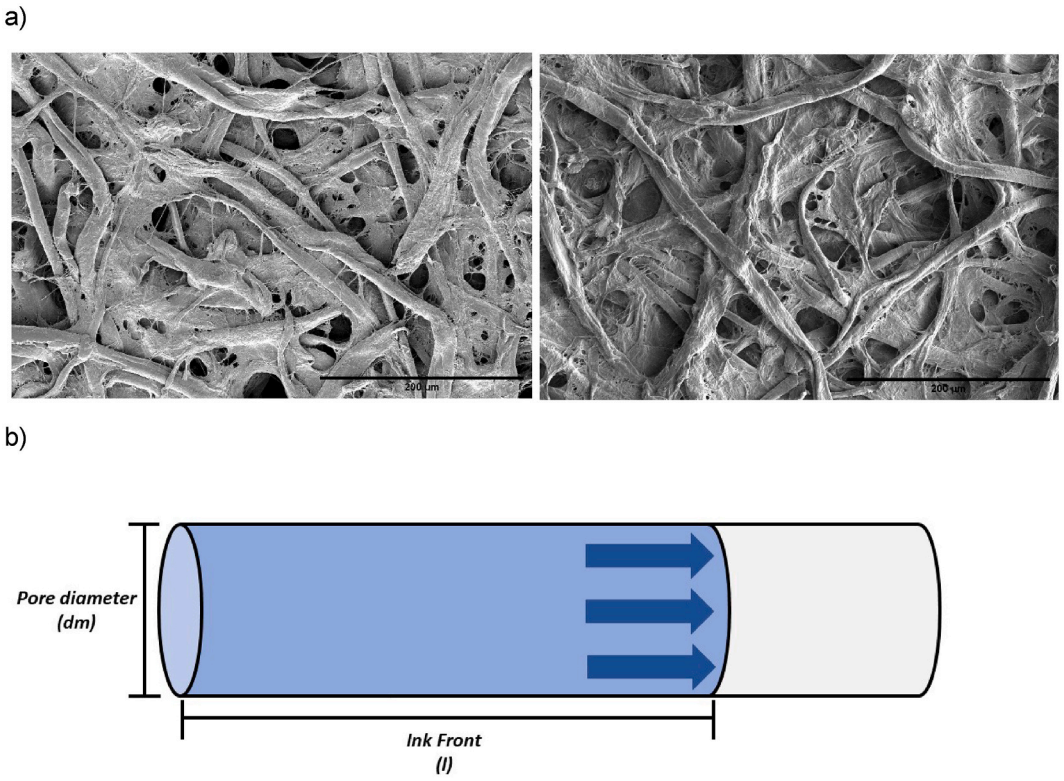

Fig. 2. (**a**) SEM images of the morphology of untreated 3MM chromatography paper (200 µm scale) and (**b**) schematic representation of the paper fibers as capillary tubes.

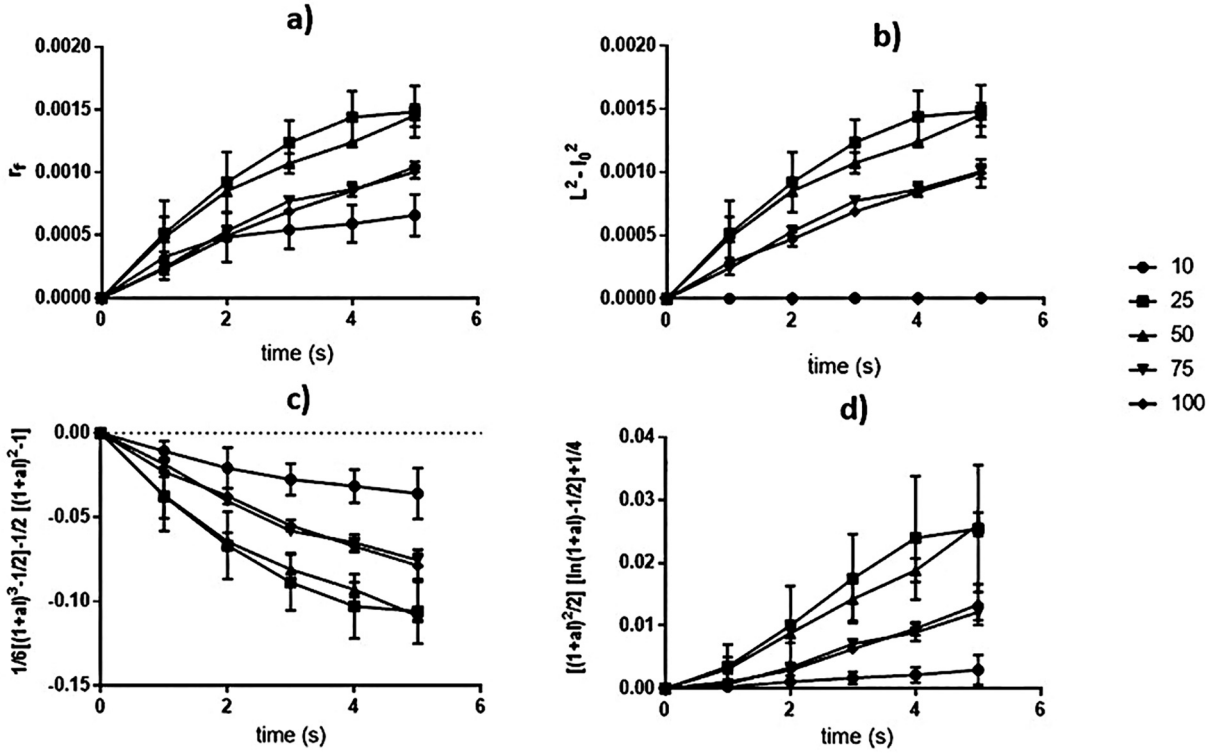

Fig. 3. Variation with time of ink flow-related parameters used for the mathematical fitting of four ink models (% *v*/v as shown in labels) to: (**a**) hemispherical flow, (**b**) upward wicking, (**c**) cylindrical flow, and (**d**) spherical flow equations.

Table 3
Theoretical permeability and mathematical fitting models for the radial penetration of the ink models in Whatman 3MM Chr paper.

Ink Conc. (%, v/v)	Theoretical Permeability[I] Kozeny-Karman Model Variations			Radial immbibition[II] [29]			Upward Wicking[III] [30]			Cylindrical flow (Sector-shaped porous media)[IV] [31]			Spherical flow (Hemispherical porous media)[IV] [31]		
	$K = r^2\frac{\varepsilon}{4k}$ [30]	$K = \frac{dm^2}{36k}\frac{\varepsilon^3}{(1-\varepsilon)^2}$ [36]	$K = \frac{dm^2}{180}\frac{\varepsilon^3}{(1-\varepsilon)^2}$ [29]	$r_f = A^{1/3}t^{1/3}$ $K = \frac{A^3\mu}{3p_c r_0}$			$L^2 - l_0^2 = a^2(t-t_0)$ $K = \frac{a^2\mu\varepsilon}{2p_c}$			$\frac{(1+al)^2}{2}\left[ln(1+al) - \frac{1}{2}\right] + \frac{1}{4} = a^2Dt$ $K = \frac{h^2}{12}$			$\frac{1}{6}\left[(1+al)^3 - \frac{1}{2}\right] - \frac{1}{2}\left[(1+al)^2 - 1\right] = a^2Dt$ $K = \frac{h^2}{12}$		
	(m^2)	(m^2)	(m^2)	A ($m/s^{1/3}$)	r^2	K (m^2)	D (m^2/s)	r^2	K (m^2)	D (m^2/s)	r^2	K (m^2)	D (m^2/s)	r^2	K (m^2)
10	2.38×10^{-12}	3.10×10^{-11}	2.63×10^{-11}	3.66×10^{-4}	0.9110	2.17×10^{-16}	1.62×10^{-6}	0.9127	5.52×10^{-14}	2.74×10^{-8}	0.9167	1.22×10^{-18}	-3.94×10^{-7}	0.9072	2.52×10^{-16}
25	2.38×10^{-12}	3.10×10^{-11}	2.63×10^{-11}	5.79×10^{-4}	0.9525	9.99×10^{-16}	3.50×10^{-4}	0.8735	1.61×10^{-11}	2.55×10^{-7}	0.9593	1.92×10^{-16}	-1.19×10^{-6}	0.8875	4.19×10^{-15}
50	2.38×10^{-12}	3.10×10^{-11}	2.63×10^{-11}	7.48×10^{-4}	0.9117	3.07×10^{-15}	2.96×10^{-4}	0.9363	1.80×10^{-11}	2.19×10^{-7}	0.9715	2.51×10^{-16}	-1.08×10^{-6}	0.8835	6.12×10^{-15}
75	2.38×10^{-12}	3.10×10^{-11}	2.63×10^{-11}	5.07×10^{-4}	0.8531	1.40×10^{-15}	2.22×10^{-4}	0.9508	1.97×10^{-11}	9.98×10^{-8}	0.9456	1.20×10^{-16}	-7.25×10^{-7}	0.9494	5.91×10^{-15}
100	2.38×10^{-12}	3.10×10^{-11}	2.63×10^{-11}	5.03×10^{-4}	0.8715	2.49×10^{-15}	2.18×10^{-4}	0.9720	3.43×10^{-11}	9.33×10^{-8}	0.9331	3.02×10^{-16}	-6.60×10^{-7}	0.9706	1.51×10^{-14}

[I] *dm=diameter of pores (13.86 ± 4.14 μm), ε=porosity (0.8441 ± 0.04), k = 4.246, r=dm/2;* [II] $p_c = 2\gamma cos\Theta/r$; [III] $p_c = 2\gamma/r$; [IV] h = (D*6 μ)/(Υ cosΘ).

Washburn model establishes that large pores filled more rapidly than small pores, which has been contradicted as inertia and viscosity are suggested to play a main role during mathematical modelling [16]. As denoted in Section 3.2, the development of Lucas-Washburn equation into a model for upward wicking resulted in the high approximation of the permeability values to the theoretically determined ones by the Kozeny-Karman model. Data fitting ($t \leq 5$ s) was carried out for Lucas-Washburn equations as a linear model (eqs. 13 and 14) to assess either their disadvantages or their adequate fitting to 3MM chromatography paper, as already discussed by some authors [16,41]. Equation fitting was performed as shown in the displayed curves in Fig. 4a and Fig. 4b, from which the fitted *D* values were obtained and reported in Table 4. As shown in eq. 13, when Poiseuille flow and the wetting force are considered, Lucas-Washburn equation denotes the imbibition length as a function of the square root of time in increments regulated by the surface tension, dynamic viscosity of the ink model, the contact angle between the ink and the paper matrix, along with the pore radius of the paper fibers expressed as capillary tubes [24]. Despite the high determination coefficients (r^2), the fitted *D* values were not comparable with the expected calculations when integrating the physicochemical parameters of both the ink models and the paper matrix. On the other hand, spontaneous imbibition triggered by inertial effects can be described by modifying Lucas-Washburn model with Bosanquet model, in which the penetration length is directly proportional to the imbibition time (eq. 14), mainly controlled by the density value (inertial regime) [24]. Similar to the observed outcome in the first fitting, even when the fitted results resulted in high r^2 values, their magnitudes were not close enough to the expected numbers. Both results coincided with the reported behavior in wicking, where neither Lucas-Washburn nor Bosanquet adaptation were sufficient for its full characterization [24]. In light of these pitfalls, another simplified model for explaining the kinetics of

Fig. 4. Theoretical (dashed lines) and experimental approximations (plotted points) of the imbibition length by Lucas-Washburn model after data fitting to (**a**) eq. 13 and (**b**) eq. 14. Each symbol corresponds to the indicated ink model.

Table 4
Comparison of the fitted and expected data for Lucas-Washburn equation as a linear expression.

	$l^2 = D * t$				$l = D * t$		
Ink Concentration (%, v/v)	D (m^2/s)	r^2	Expected [I] $D = \frac{r\gamma\cos\theta}{2\mu}$	Marmur Model[II] $K = \frac{C}{S^2}\frac{\varepsilon^3}{(1-\varepsilon)^2}$	D (m/s)	r^2	Expected[III] $D = \left(\frac{2\gamma\cos\theta}{r\rho}\right)^{0.5}$
10	5.35×10^{-8}	0.84	1.48969×10^{-4}	1.82×10^{-15}	1.13×10^{-4}	0.91	3.91
25	4.78×10^{-7}	0.96	1.10211×10^{-4}	2.20×10^{-14}	3.50×10^{-4}	0.87	3.68
50	3.99×10^{-7}	0.97	8.31481×10^{-5}	2.43×10^{-14}	2.96×10^{-4}	0.94	3.72
75	1.91×10^{-7}	0.95	5.6538×10^{-5}	1.71×10^{-14}	2.21×10^{-4}	0.95	3.68
100	1.52×10^{-7}	0.94	3.22162×10^{-5}	2.39×10^{-14}	2.19×10^{-4}	0.97	3.44

[I] γ = *interfacial surface tension*, μ = *dynamic viscosity*, $\theta = 0$; [II] $C = DS(1-\varepsilon)\mu/2\varepsilon\gamma\cos\theta$, $S = 2\varepsilon/r(1-\varepsilon)$, $r = 6.93$ μm, ε = *porosity (0.8441 ± 0.04)*; [III] $r = 6.93$ μm, ρ = *density*.

liquid capillary penetration in porous media developed by Marmur [38] was evaluated. In this case, a larger sample volume implied the integration of the gravitational effects on a transformed version of Lucas-Washburn by integrating Darcy's law rather than Poiseuille equation. Its nongravitational expression, similar to Eq. 13 ($l^2 = D*t$), was solved by applying the fitted D values and physicochemical parameters, to obtain C, S as well as the corresponding Kozeny-Karman permeability (Table 4), according to eqs. 15, 16 and 17.

$$D = \frac{2C\varepsilon\gamma\cos\theta}{S(1-\varepsilon)\mu} \tag{15}$$

$$K = \frac{C}{S^2}\frac{\varepsilon^3}{(1-\varepsilon)^2} \tag{16}$$

$$S = \frac{2\varepsilon}{r(1-\varepsilon)} \tag{17}$$

Where ε is the porosity, $\theta = 0$, r is the pore radius, γ the interfacial surface tension, and μ is the dynamic viscosity. Regardless of the promising approach proposed by Marmur, as noted in Fig. S7, the calculated permeability was not equivalent to any experimental or theoretical values previously determined in this work.

Therefore, apart from the diffusive behavior confirmed for a cylindric geometry, upward wicking can be considered for studying the radial imbibition in 3MM chromatography paper. In this regard, imbibition in cellulose fibers occurs by absorption in their internal cavities as well as the inter-fiber pores within the fibrous network [46]. However, as previously studied [41], the application of Lucas-Washburn model is commonly accompanied by the assumption of pore saturation behind the ink front and pore uniformity [46], which in this work were accomplished by looking at the fibers as homogenous capillary tubes for a modified version of Lucas-Washburn for upward wicking, in which the large ink volume allowed the pore saturation behind the wetting front.

4. Conclusion

The equation for the diffusion in a cylinder, fitted in this work, allowed the description of all the data until a steady state was reached, with satisfactory correlation values. On the other hand, comparison of theoretically and experimentally based permeability values indicated that the model for upward wicking was the best descriptor for the capillary movement of a model substance in a porous thin substrate. This study enabled the characterization of the performance of 3MM chromatography paper used as a biosensing support matrix [32], by using ink as a surrogate model of the flow of small molecules (e.g. mycotoxins) and colloidal particles. In keeping with previous studies at a small scale, the application of Lucas-Washburn equation for the description of the front distance at a microscale had null correlation to the experimental front radius, thus confirming the drawbacks from this general model. Nevertheless, our study enabled the characterization of both regimes, where a diffusive and non-diffusive spreading was simultaneously confirmed through the proximity of the experimental data with its theoretical determinations. A better understanding of the fundamental phenomena governing the transport of small molecules in paper substrates is important in the development of future biosensing applications.

Declaration of Competing Interest

Hereby we declare that we have not conflict of interests of any kind related to our submitted manuscript.

Acknowledgments

V. Mirón-Mérida received a scholarship from CONACyT.

Supplementary data

Supplementary data to this article can be found online at https://doi.org/10.1016/j.sbsr.2021.100421.

References

[1] J. Cai, L. You, X. Hu, J. Wang, R. Peng, Prediction of effective permeability in porous media based on spontaneous imbibition effect, Int. J. Modern Physics C 23 (2012) 1250054, https://doi.org/10.1142/S0129183112500544.
[2] J. Cai, X. Hu, D.C. Standnes, L. You, An analytical model for spontaneous imbibition in fractal porous media including gravity, Colloids Surf. A Physicochem. Eng. Asp. 414 (2012) 228–233, https://doi.org/10.1016/j.colsurfa.2012.08.047.
[3] S. Suo, M. Liu, Y. Gan, Modelling imbibition processes in heterogeneous porous media, Transp. Porous Media 126 (2019) 615–631, https://doi.org/10.1007/s11242-018-1146-7.
[4] L. Liu, D. Yang, G. Liu, Signal amplification strategies for paper-based analytical devices, J. Biosens. Bioelectron. 136 (2019) 60–75, https://doi.org/10.1016/j.bios.2019.04.043.
[5] J. Moon, G. Kim, S. Lee, A gold nanoparticle and aflatoxin B1-BSA conjugates based lateral flow assay method for the analysis of aflatoxin B1, Materials. 5 (2012) 634–643, https://doi.org/10.3390/ma5040634.
[6] S. Lee, G. Kim, J. Moon, Performance improvement of the one-dot lateral flow immunoassay for aflatoxin B1 by using a smartphone-based reading system, Sensor. 13 (2013) 5109–5116, https://doi.org/10.3390/s130405109.
[7] S. Yu, L. He, F. Yu, L. Liu, C. Qu, L. Qu, J. Liu, Y. Wu, Y. Wu, A lateral flow assay for simultaneous detection of deoxynivalenol, fumonisin B1 and aflatoxin B1, Toxicon. 156 (2018) 23–27, https://doi.org/10.1016/j.toxicon.2018.10.305.
[8] S. Dalirirad, A.J. Steckl, Aptamer-based lateral flow assay for point of care cortisol detection in sweat, Sens. Actuat. B: Chem. 283 (2019) 79–86, https://doi.org/10.1016/j.snb.2018.11.161.
[9] A. Pesenti, R.V. Taudte, B. McCord, P. Doble, C. Roux, L. Blanes, Coupling paper-based microfluidics and lab on a chip technologies for confirmatory analysis of trinitro aromatic explosives, Anal.Chem. 86 (2014) 4707–4714, https://doi.org/10.1021/ac403062y.
[10] T.M.G. Cardoso, P.T. Garcia, W.K.T. Coltro, Colorimetric determination of nitrite in clinical, food and environmental samples using microfluidic devices stamped in paper platforms, Anal.Methods. 7 (2015) 7311–7317, https://doi.org/10.1039/C5AY00466G.
[11] W. Liu, J. Kou, H. Xing, B. Li, Paper-based chromatographic chemiluminescence chip for the detection of dichlorvos in vegetables, Biosens. Bioelectron. 52 (2014) 76–81, https://doi.org/10.1016/j.bios.2013.08.024.
[12] X. Zhang, Z. Wang, Y. Fang, R. Sun, T. Cao, N. Paudyal, W. Fang, H. Song, Antibody microarray immunoassay for simultaneous quantification of multiple mycotoxins in corn samples, Toxins. 10 (2018) 415, https://doi.org/10.3390/toxins10100415.

[13] H. Duan, Y. Li, Y. Shao, X. Huang, Y. Xiong, Multicolor quantum dot nanobeads for simultaneous multiplex immunochromatographic detection of mycotoxins in maize, Sensors Actuators B Chem. 291 (2019) 411–417, https://doi.org/10.1016/j.snb.2019.04.101.
[14] R.F. Carvalhal, M.S. Kfouri, M.H.O. Piazetta, A.L. Gobbi, L.T. Kubota, Electrochemical detection in a paper-based separation device, Anal. Chem. 82 (2010) 1162–1165, https://doi.org/10.1021/ac902647r.
[15] 12 Y. Wang, J. Sun, Y. Hou, C. Zhang, D. Li, H. Li, M. Yang, C. Fan, B. Sun, A SERS-based lateral flow assay biosensor for quantitative and ultrasensitive detection of interleukin-6 in unprocessed whole blood. 2019, Biosens. Bioelectron. 141 (2019) 111432, https://doi.org/10.1016/j.bios.2019.111432.
[16] H. Aslannejad, H. Fathi, S.M. Hassanizadeh, A. Raoof, N. Tomozeiu, Movement of a liquid droplet within a fibrous layer: direct pore-scale modeling and experimental observations, Chem. Eng. Sci. 191 (2018) 78–86, https://doi.org/10.1016/j.ces.2018.06.054.
[17] J. Kettle, T. Lamminmäki, P. Gane, A review of modified surfaces for high speed inkjet coating, Surf. Coat. Technol. 204 (2010) 2103–2109, https://doi.org/10.1016/j.surfcoat.2009.10.035.
[18] T.T. Lamminmäki, J.P. Kettle, P.J.T. Puukko, P.A.C. Gane, The chromatographic separation of anionic dye in inkjet coating structures, Colloids Surf. A Physicochem. Eng. Asp. 377 (2011) 304–311, https://doi.org/10.1016/j.colsurfa.2011.01.026.
[19] T.T. Lamminmäki, J.P. Kettle, P.J.T. Puukko, C.J. Ridgway, P.A.C. Gane, Short timescale inkjet ink component diffusion: an active part of the absorption mechanism into inkjet coatings, J. Colloid Interface Sci. 365 (2012) 222–235, https://doi.org/10.1016/j.jcis.2011.08.045.
[20] X. Wang, J.A. Hagen, I. Papautsky, Paper pump for passive and programmable transport, Biomicrofluidics. 7 (2013), 014107, https://doi.org/10.1063/1.4790819.
[21] D. Shou, L. Ye, J. Fan, K. Fu, M. Mei, H. Wang, Q. Chen, Geometry-induced asymmetric capillary flow, Langmuir. 30 (2014) 5448–5454, https://doi.org/10.1021/la500479e.
[22] A. Borhan, K.K. Rungta, An experimental study of the radial penetration of liquids in thin porous substrates, J. Colloid Interface Sci. 158 (1993) 403–411, https://doi.org/10.1006/jcis.1993.1272.
[23] M.A. Mahmud, E.J.M. Blondeel, M. Kaddoura, B.D. MacDonald, Features in microfluidic paper based devices made by laser cutting: how small can they be? Micromachines. 9 (2018) 220, https://doi.org/10.3390/mi9050220.
[24] G. Liu, S. Fu, Z. Lu, M. Zhang, C. Ridgway, P. Gane, Contrasting liquid imbibition into uncoated versus pigment coated paper enables a description of imbibition into new-generation surface-filled paper, Eur. Phys. J. E. 40 (2017) 1–11, https://doi.org/10.1140/epje/i2017-11600-y.
[25] Y. Shi, M.R. Yassin, H. Dehghanpour, A modified model for spontaneous imbibition of wetting phase into fractal porous media, Colloids Surf. A Physicochem. Eng. Asp. 543 (2018) 64–75, https://doi.org/10.1016/j.colsurfa.2017.12.052.
[26] A. Abadian, S.S. Manesh, S.J. Ashtiani, Hybrid paper-based microfluidics: combination of paper-based analytical device (μPAD) and digital microfluidics (DMF) on a single substrate, Microfluid. Nanofluid. 21 (2017) 65, https://doi.org/10.1007/s10404-017-1899-2.
[27] H. Aslannejad, S.V. Loginov, B. van der Hoek, E.M. Schoonderwoerd, H. C. Gerritsen, S.M. Hassanizadeh, Liquid droplet imbibition into a thin coating layer: direct pore-scale modeling and experimental observations, Prog. Org. Coat. 151 (2021) 106054, https://doi.org/10.1016/j.porgcoat.2020.106054.
[28] C.Z. Qin, H. van Brummelen, A dynamic pore-network model for spontaneous imbibition in porous media, Adv. Water Resour. 133 (2019) 103420, https://doi.org/10.1016/j.advwatres.2019.103420.
[29] J. Xiao, H.A. Stone, D. Attinger, Source-like solution for radial imbibition into a homogeneous semi-infinite porous medium, Langmuir. 28 (2012) 4208–4212, https://doi.org/10.1021/la204474f.
[30] G. Callegari, I. Tyomkin, K.G. Kornev, A.V. Neimark, Y.L. Hsieh, Absorption and transport properties of ultra-fine cellulose webs, J. Colloid Interface Sci. 353 (2011) 290–293, https://doi.org/10.1016/j.jcis.2010.09.015.
[31] E. Elizalde, R. Urteaga, C.L.A. Berli, Rational design of capillary-driven flows for paper-based microfluidics, Lab Chip 15 (10) (2015) 2173–2180. https://doi.org/10.1039/C4LC01487A.
[32] V.A. Mirón-Mérida, M. Wu, Y.Y. Gong, Y. Guo, M. Holmes, R. Ettelaie, F. M. Goycoolea, Genipin cross-linked chitosan for signal enhancement in the colorimetric detection of aflatoxin B1 on 3MM chromatography paper, Sens. Bio-Sens. Res. 29 (2020) 100339.20, https://doi.org/10.1016/j.sbsr.2020.100339.
[33] E.F. Gabriel, P.T. Garcia, T.M. Cardoso, F.M. Lopes, F.T. Martins, W.K. Coltro, Highly sensitive colorimetric detection of glucose and uric acid in biological fluids using chitosan-modified paper microfluidic devices, Analyst 141 (2016) 4749–4756, https://doi.org/10.1039/C6AN00430J.
[34] J. Guan, K.L. Fujimoto, M.S. Sacks, W.R. Wagner, Preparation and characterization of highly porous, biodegradable polyurethane scaffolds for soft tissue applications, Biomaterials. 26 (2005) 3961–3971, https://doi.org/10.1016/j.biomaterials.2004.10.018.
[35] J. Crank, The Mathematics of Diffusion, second ed., Oxford University Press, Bristol, 1979.
[36] P. Xu, B. Yu, Developing a new form of permeability and Kozeny–Carman constant for homogeneous porous media by means of fractal geometry, Adv. Water Resour. 31 (2008) 74–81, https://doi.org/10.1016/j.advwatres.2007.06.003.
[37] O. Rahli, L. Tadrist, M. Miscevic, R. Santini, Fluid flow through randomly packed monodisperse fibers: the Kozeny-Carman parameter analysis, J. Fluids Eng. 119 (1997) 188–192, https://doi.org/10.1115/1.2819107.
[38] A. Marmur, Kinetics of penetration into uniform porous media: testing the equivalent-capillary concept, Langmuir. 19 (2003) 5956–5959, https://doi.org/10.1021/la034490v.
[39] Z. Yang, G. Xu, J. Reboud, S.A. Ali, G. Kaur, J. McGiven, N. Boby, P.K. Guptam, P. Chaudhuri, J.M. Cooper, Rapid veterinary diagnosis of bovine reproductive infectious diseases from semen using paper-origami DNA microfluidics, ACS Sens. 3 (2018) 403–409, https://doi.org/10.1021/acssensors.7b00825.
[40] E.M. Schoonderwoerd, E. M. Modelling the imbibition of an ink-like fluid into the thin coating layer of paper (Master's thesis), second ed., Utrecht University Repository, Utrecht, Netherlands, 2019.
[41] E. Elizalde, R. Urteaga, C.L.A. Berli, Precise capillary flow for paper-based viscometry, Microfluid. Nanofluid. 20 (2016) 135, https://doi.org/10.1007/s10404-016-1800-8.
[42] D. Topgaard, O. Söderman, Diffusion of water absorbed in cellulose fibers studied with 1H-NMR, Langmuir. 17 (2001) 2694–2702, https://doi.org/10.1021/la000982l.
[43] E. Evans, E.F.M. Gabriel, W.K.T. Coltro, C.D. Garcia, Rational selection of substrates to improve color intensity and uniformity on microfluidic paper-based analytical devices, Analyst. 139 (2014) 2127–2132, https://doi.org/10.1039/C4AN00230J.
[44] I.A. Balakhnina, N.N. Brandt, A.Y. Chikishev, I.M. Pelivanov, N.L. Rebrikova, Optoacoustic measurements of the porosity of paper samples with foxings, Appl. Phys.Lett. 101 (2012) 174101, https://doi.org/10.1063/1.4761984.
[45] J. Songok, M. Toivakka, Enhancing capillary-driven flow for paper-based microfluidic channels, ACS Appl. Mater. Interfaces 8 (2016) 30523–30530, https://doi.org/10.1021/acsami.6b08117.
[46] S. Chang, J. Seo, S. Hong, D.G. Lee, W. Kim, Dynamics of liquid imbibition through paper with intra-fibre pores, J. Fluid Mech. 845 (2018) 36–50, https://doi.org/10.1017/jfm.2018.235.